Ag_2O/TiO_2 Nanobelts Heterostructure with Enhanced Ultraviolet and Visible Photocatalytic Activity

Weijia Zhou, Hong Liu,* Jiyang Wang, Duo Liu, Guojun Du, and Jingjie Cui

State Key Laboratory of Crystal Materials, Center of Bio & Micro/Nano Functional Materials, Shandong University, 27 Shandanan Road, Jinan 250100, P. R. China

ABSTRACT Ag_2O/TiO_2 heterostructure with high photocatalytic activity both in ultraviolet and visible-light region was synthesized via a simple and practical coprecipitation method by using surface-modified TiO_2 nanobelts as substrate materials. The as-prepared heterostructure composite included Ag_2O nanoparticles assembled uniformly on the rough surface of TiO_2 nanobelts. Comparing with pure TiO_2 nanobelts and Ag_2O nanoparticles, the composite photocatalyst with a wide weight ratio between TiO_2 and Ag_2O exhibited enhanced photocatalytic activity under ultraviolet and visible light irradiation in the decomposition of methyl orange (MO) aqueous solution. On the basis of the characterization by X-ray diffraction, photoluminescence and UV−vis diffuse reflectance spectroscopies, two mechanisms were proposed to account for the photocatalytic activity of Ag_2O/TiO_2 nanobelts' heterostructure.

KEYWORDS: TiO_2 nanobelts • Ag_2O/TiO_2 heterostructure • photocatalytic activity • electron capture agent • visible-light photocatalysis

INTRODUCTION

Titanium dioxide (TiO_2) has been intensively investigated as a semiconductor photocatalyst since Fujishima and Honda discovered the photocatalytic splitting of water on TiO_2 electrodes in 1972 (1). Recently, the application of TiO_2 photocatalysts has mainly been focused on the decomposing toxic and hazardous organic pollutants in contaminated air and water, which is of great importance for the environmental protection (2−5). Although notable advances have been made, the high recombination rate of the photogenerated electron/hole pairs hinders its further application in industry. When TiO_2 is exposed to UV light, electrons in the uppermost valence band will jump to the conduction band and create conduction band electrons and valence band holes. In most instances, the valence band holes and conduction band electrons simply recombine liberating heat or light, a process known as recombination. Recombination is responsible for the low quantum yields. Photoelectron trapping has long been regarded as an effective mechanism to reduce the charge recombination on semiconductor photocatalysts. Numerous studies have suggested that fine particles of transition metals or their oxides dispersed on the surface of a photocatalyst matrix can act as electron traps on photocatalyst to improve its photocatalytic activity (6−10). In an ideal system, the quantum yield is proportional to the rate of the charge transfer and inversely proportional to the sum of the charge-transfer rate and the electron hole recombination rate. Coating TiO_2 nanoparticles on an electrode, which is based with a positive charge, can suppress the rate of hole-electron recombination because the electrode can act as a sink for the photogenerated electrons (11). Although this application has achieved some degree of success, the true potential of the process is not fully realized, because the resistance path for the electrons is relatively long and the surface area for reaction is low. The other main drawback of TiO_2 photocatalyst in practical application is the lack of visible light utilization because of a large band gap in TiO_2 (3.2 eV for the anatase phase and 3.0 eV for the rutile phase). To handle this problem, numerous studies have recently been performed to enhance the photocatalytic efficiency and visible light utilization of TiO_2, which include impurity doping (12−15), metallization (16, 17), and sensitization (18−21). In addition, recovery and reutilization of photocatalyst is also urgent to be solved. Removal of TiO_2 particles, such as P-25, from large volumes of water following photocatalytic process is problematic due to their nano-size (22). So, it is of great significance to develop TiO_2 photocatalyst with a segregative sepeciality that can be used in both UV irradiation (290−400 nm) and visible light (400−700 nm) to enhance the photocatalysis efficiency (23, 24).

Here, we found a new system of Ag_2O/TiO_2 nanobelts, which can effectively suppress the rate of hole-electron recombination under UV light irradiation. At the same time, the Ag_2O/TiO_2 heterostructure also has a high visible photocatalytic activity. Loading of noble metal particles, such as platinum (25), gold (26), and palladium (27), on TiO_2 photocatalysts can improve photocatalytic activities. Especially, the deposition of Ag nanoparticles on TiO_2 photocatalyst can highly improve its photocatalytic efficiency through the schottky barrier conduction band electron trapping and consequent longer electron-hole pair lifetimes (28−31).

* Corresponding author. E-mail: hongliu@sdu.edu.cn.
Received for review May 5, 2010 and accepted July 9, 2010

DOI: 10.1021/am100394x

However, there were few reports about Ag_2O nanoparticles of application in TiO_2 photocatalysis (32, 33). Ag_2O particles are commonly used as water cleaning agent, colorant and catalyst (34). In this paper, we demonstrate that Ag_2O nanoparticles can be used as an efficient electron absorbing agent under UV light irradiation and as an efficient photosensitiser under visible light irradiation in Ag_2O/TiO_2 coordinated photocatalysis system. Ag_2O nanoparticles were loaded on the surface of TiO_2 nanobelts by a simply coprecipitation to form Ag_2O/TiO_2 heterostructure. Here, TiO_2 nanobelts were chosen as the test material, because one-dimensional nanostructures have advantages over nanoparticles, such as enhanced visible-light scattering and absorption, rapid diffusion-free electron transport along the long direction; and the low number of grain boundaries. The photocatalytic activity of Ag_2O/TiO_2 nanobelts driven by UV and visible light was investigated via the photocatalytic decomposition of methyl orange (MO). The two different photocatalytic mechanisms of Ag_2O/TiO_2 under UV- and visible-light irradiation were illustrated and discussed.

EXPERIMENTAL SECTION

Materials. Titania P-25 (TiO_2; ca. 80% anatase, and 20% rutile), sodium hydroxide (NaOH), hydrochloric acid (HCl), sulfuric acid (H_2SO_4), and silver nitrate ($AgNO_3$) were purchased from China National Medicines Corporation Ltd. All chemicals were analytical grade without further purification. Deionized water was used throughout this study.

Preparation of Photocatalysts. ***TiO_2 Nanobelts.*** Titanate nanobelts were synthesized by the hydrothermal process in concentrated NaOH aqueous solution. A commercial titania P-25 was used as the precursor, and a typical process is as follows: 0.1 g precursor was mixed with 20 mL of 10 M NaOH aqueous solution, followed by hydrothermal treatment at 180 °C in a 25 mL Teflon-lined autoclave for 72 h. The treated powder was washed thoroughly with deionized water followed by a filtration and drying process. The sodium titanate nanobelts were obtained. These were immersed in 0.1 M HCl aqueous solution for 24 h and then washed thoroughly with water to get hydrogen titanate nanobelts. The obtained H-titanate nanobelts were added into a 25 mL Teflon vessel, then filled 0.02 M H_2SO_4 aqueous solution up to 80% of the total volume and maintained at 100 °C for 12 h. Finally, the products were isolated from the solution by centrifugation and sequentially washed with deionized water for several times, and dried at 70 °C for 10 h. By annealing the hydrogen titanate obtained by acid corrosion at 600 °C for 1 h, we obtained anatase TiO_2 nanobelts with rough surfaces.

Ag_2O/TiO_2 Nanobelt Heterostructure. Ag_2O/TiO_2 heterostructure with different weight ratio ranging from 10:1 to 1:10 were prepared by the precipitation method. A typical process of Ag_2O/TiO_2 nanobelts at the weight ratio of 1:1 is as follows: 0.2 g of TiO_2 nanobelts was dispersed in 50 mL of distilled water, and 0.29 g of $AgNO_3$ was added to the suspension. The mixture was stirred magnetically for 30 min. 50 mL of 0.2 M NaOH was dropped to the above mixture of $AgNO_3$ and TiO_2. The amount of NaOH was more than sufficient to precipitate Ag_2O from the added $AgNO_3$, and the final pH 14. Finally, TiO_2 nanobelts coated by Ag_2O nanoparticles were washed thoroughly with deionized water followed by a filtration and drying process. The pure Ag_2O nanoparticles were synthesized from $AgNO_3$ and NaOH aqueous solution by the precipitation method, which was used as the blank sample.

Characterization of Catalysts. X-ray powder diffraction (XRD) pattern of catalysts were recorded on a Bruke D8 Advance powder X-ray diffractometer with Cu Kα ($\lambda = 0.15406$ nm). HITACHI S-4800 field-emission scanning electron microscope (FE-SEM) was used to characterize the morphologies and size of the synthesized Ag_2O/TiO_2 samples. The chemical composition was investigated via energy-dispersive X-ray spectroscopy (EDS). High-resolution transmission electron microscopy (HRTEM) images were carried out with a JOEL JEM 2100 microscope. Photoluminescence (PL) spectra were recorded via a FLS920 fluorescence spectrometer with an excitation wavelength of 380 nm. UV-Vis diffuse reflectance spectra (DRS) of the samples were recorded on a UV-Vis spectrophotometer (UV-2550, Shimadzu) with an integrating sphere attachment. The analyzed range was 200−650 nm, and $BaSO_4$ was used as a reflectance standard. The test results without explanation in the paper are for the samples with a weight ratio of 1:1.

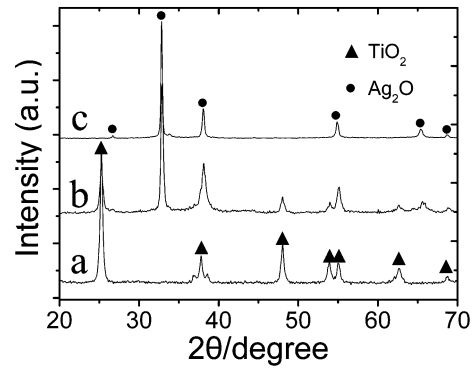

FIGURE 1. XRD patterns of the as-synthesized products: (a) TiO_2 nanobelts, (b) Ag_2O/TiO_2 heterostructure, and (c) Ag_2O nanoparticles.

Photocatalytic Degradation of MO under UV and Visible-Light Irradiation. Methyl orange (MO) was selected as model chemicals to evaluate the activity and properties of the Ag_2O/TiO_2 photocatalyst. In a typical experiment, 20 mL aqueous suspensions of MO (20 mg/L) and 20 mg of Ag_2O/TiO_2 photocatalyst powders were placed in a 50 mL beaker. Prior to irradiation, the suspensions were magnetically stirred in the dark for 30 min to establish adsorption/desorption equilibrium between the dye and the surface of the catalyst under room air equilibrated conditions. A 20 W UV lamp with a maximum emission at 254 nm was used as the UV resource for UV light photocatalysis. A 300 W Xe arc lamp was used as the visible light source for visible-light photocatalysis. At given irradiation time intervals, the mixed solution were collected and centrifuged to remove the catalyst particulates for analysis. The residual MO concentration was detected using a UV−vis spectrophotometer (Hitachi UV-3100).

RESULTS AND DISCUSSION

XRD patterns of TiO_2 nanobelts, Ag_2O nanoparticles and Ag_2O/TiO_2 heterostructure are shown in Figure 1. All the diffraction peaks in the pattern of pure TiO_2 nanobelts can be indexed as anatase type structure (Figure 1a), and all the diffraction peaks in the pattern of pure Ag_2O nanoparticles correspond to the cubic structure (Figure 1c). The anatase TiO_2 and Ag_2O phases coexist in the Ag_2O/TiO_2 heterostructure crystals, and the XRD patterns match their JCPDS files nos. 21−1272 and 41−1104, respectively (Figure 1b). In comparison with the diffraction profile of TiO_2 nanobelts, the peaks of Ag_2O nanoparticles are rather sharp, which indicates they have a relatively high degree of crystallinity.

The morphology and microstructural details of as-prepared TiO_2 nanobelts, Ag_2O nanoparticles and TiO_2 nano-

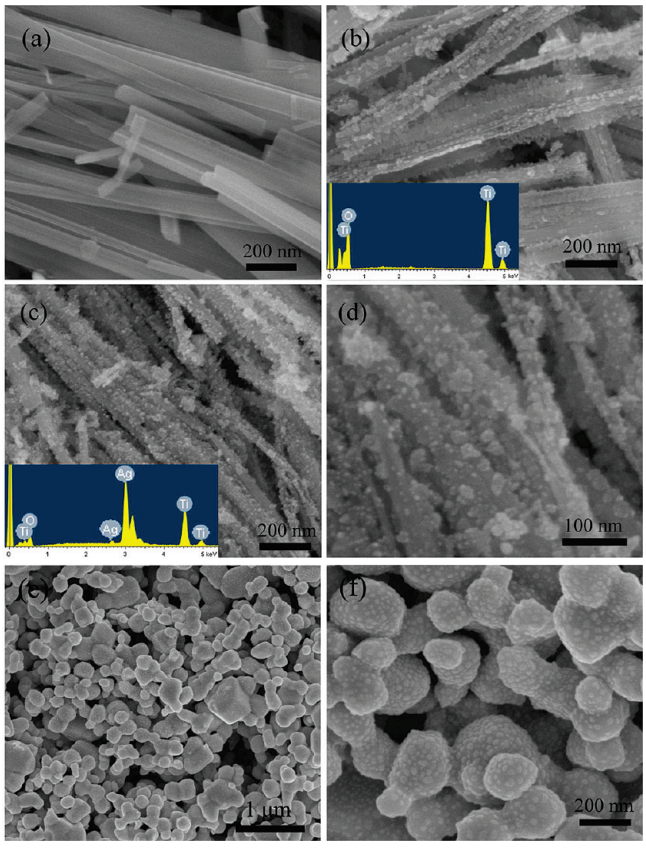

FIGURE 2. Typical SEM images of (a) TiO_2 nanobelts, (b) TiO_2 nanobelts treated with acid corrosion, (c, d) Ag_2O/TiO_2 nanobelts, and (e, f) Ag_2O nanoparticles with different magnification.

belts-coated Ag_2O were investigated by SEM and HRTEM observation. Figure 2a shows a typical SEM image of the as-prepared TiO_2 nanobelts, which has widths of 50 to 200 nm, and lengths of up to hundreds of micrometer. Figure 2b is a low-magnification SEM image of the TiO_2 nanobelts treated with acid corrosion, which possesses rough surface. Energy-dispersive X-ray spectroscopy (EDS) analysis (inset of Figure 2b) reveals that the nanobelts are only composed of Ti and O elements. TiO_2 nanobelts with rough surfaces provide a very good platform to absorb Ag_2O nanoparticles in high capacity during the co-precipitation process (Figure 2c, d). EDS analysis (inset of Figure 2c) reveals that Ag_2O/TiO_2 nanobelts heterostructure are composed of Ti, O and Ag elements. The Ag_2O nanoparticles on TiO_2 nanobelts have a narrow size distribution with a small size of 5−20 nm. In contrast, TiO_2 nanobelts without acid treatment exhibited a smooth surface where only a small number Ag_2O particles were absorbed (the result is given in Supporting Information 1). Images e and f in Figure 2 show the morphology of the Ag_2O nanoparticles obtained by the precipitation method. The size of Ag_2O nanoparticles is about 100−500 nm, which is much bigger than that of Ag_2O nanoparticles on TiO_2 nanobelts (shown in Figure 2d). It is likely that TiO_2 nanobelts with a rough surface provided numerous nucleation sites for the growth of Ag_2O nanoparticles, leading to homogeneous dispersion of Ag_2O nanoparticles on the TiO_2 nanobelts with a smaller size.

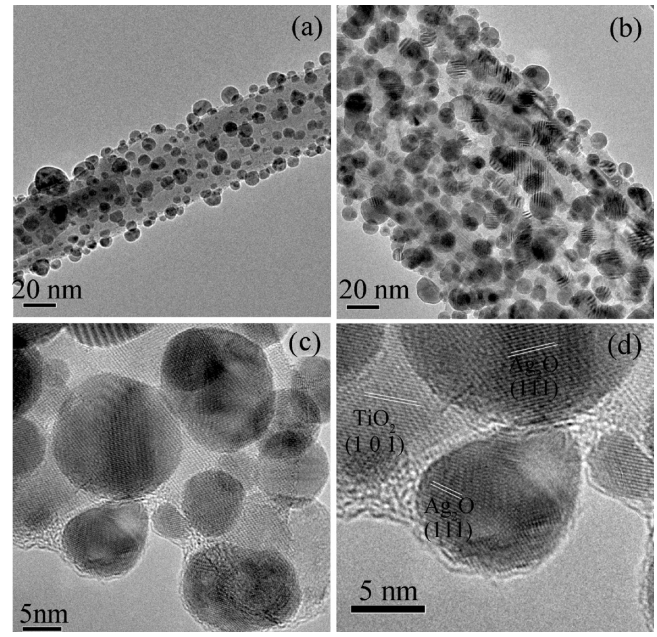

FIGURE 3. HRTEM images of Ag_2O/TiO_2 nanobelts (1:1) with different magnification.

HRTEM images of the sample further confirm the formation of a novel heterostructure between TiO_2 nanobelts and Ag_2O nanoparticles. After NaOH aqueous solution was added into the mixed aqueous solution of $AgNO_3$ and TiO_2 nanobelts, Ag_2O nanoparticles with a diameter of 5−20 nm were uniformly coated on the surface of the TiO_2 nanobelts (Figure 3a, b). It is worth noting that the Ag_2O nanoparticles on TiO_2 nanobelts are very stable and do not break off even when subjected to an ultrasonic treatment. The Ag_2O nanoparticles are tightly coupled on the surface of TiO_2 nanobelts to form Ag_2O/TiO_2 heterostructure (Figure 3c), which is propitious to electron transmission between two phases. By measuring the lattice fringes, the resolved interplanar distances are ca. 0.35 and 0.27 nm, corresponding to the (101) plane of anatase TiO_2 and the (111) plane of Ag_2O, as shown in Figure 3d. These results also suggest that the prepared sample behaved as a well-crystallized heterostructure with Ag_2O nanoparticles and TiO_2 nanobelts on nanoscale.

To evaluate the photocatalytic degradation capability of Ag_2O/TiO_2, we examined the decomposition of MO in water under UV light irradiation as a function of time (Figure 4). For comparison, the decomposition over Ag_2O nanoparticles and TiO_2 nanobelts was carried out under the same experimental conditions. As shown in Figure 4, the Ag_2O/TiO_2 heterostructure photocatalyst exhibited a high activity for MO degradation under UV irradiation. With the irradiation time increasing, the decomposition of MO dye progressed steadily and completed in 24 min of UV light irradiation. The degradation activity of Ag_2O/TiO_2 heterostructure photocatalyst was much higher than those of the Ag_2O nanoparticles and of the TiO_2 nanobelts, and the corresponding degradation rates were only 20 and 25% after the same experimental time, respectively. Via the first-order linear fit, the rate of the MO decomposition for the Ag_2O/TiO_2 heterostructure (0.017 mg/min) was more than 5-fold as fast as that of the

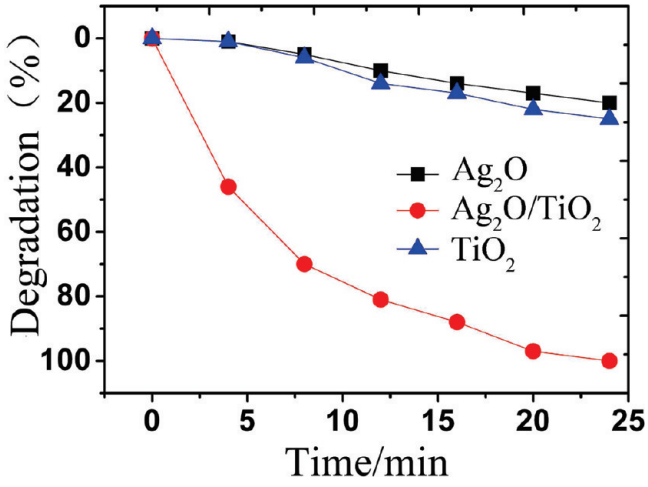

FIGURE 4. Photocatalytic degradation of MO in the presence of Ag_2O, Ag_2O/TiO_2 heterostructures, and TiO_2 nanobelts under UV light irradiation.

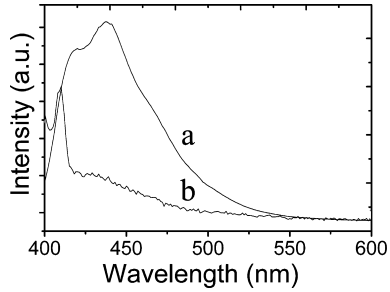

FIGURE 5. Photoluminescence (PL) spectra of (a) TiO_2 and (b) Ag_2O/TiO_2 (1:1), $\lambda_{Ex} = 380$ nm.

TiO_2 nanobelts sample (0.0034 mg/min). Although the photocatalysis activity of both Ag_2O nanoparticles and TiO_2 nanobelts are very low, the photocatalysis activity of the composite is improved greatly because of the heterostructure between Ag_2O and TiO_2.

For semiconductor nanomaterial, the PL spectra is related to the transfer behavior of the photoinduced electrons and holes, so that it can reflect the separation and recombination of photoinduced charge carriers. The PL spectra of TiO_2 nanobelts and Ag_2O/TiO_2 samples are shown in Figures 5. The excitation wavelength is determined as 380 nm, and the pure TiO_2 nanobelts have a strong emission peak at about 438 nm. The PL intensities of TiO_2 decreased with an addition of the Ag_2O. This is because Ag_2O nanoparticles deposited on the surface of TiO_2 nanobelts act as traps to capture the photoinduced electrons, and thus inhibit recombination of electron-hole pairs. The PL spectra result is consistent with the enhancement of photocatalytic activity of Ag_2O/TiO_2 nanobelts heterostructure under UV light. At the same time, the peak in spectrum b at about 409 nm is attributed to the emission peak of Ag_2O with an excitation wavelength at 380 nm.

Ag_2O/TiO_2 samples with a broad weight ratio range exhibiting high photodegradation efficiency are shown in Figure 6, and the corresponding SEM images are shown in Figure 7. The amount of the Ag_2O nanoparticles on surface of TiO_2 nanobelts increases with the increase of the Ag_2O/TiO_2 weight ratio, and the photodegradation efficiency

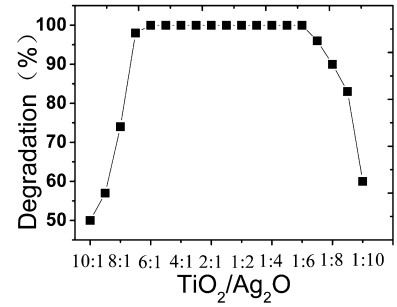

FIGURE 6. Comparisons of photocatalytic activities among the Ag_2O/TiO_2 samples with different weight ratios of TiO_2 and Ag_2O under UV light irradiation in 24 min.

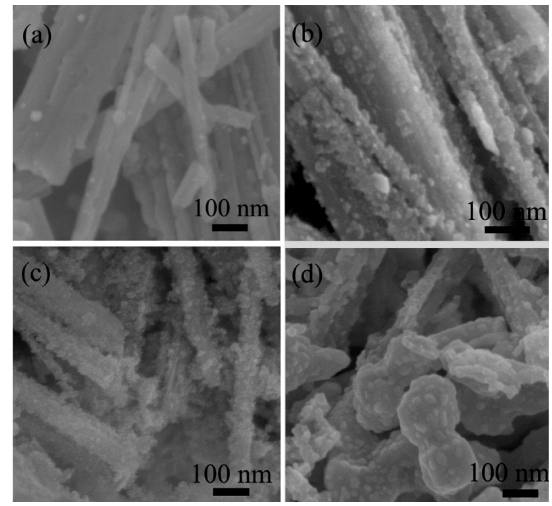

FIGURE 7. Typical SEM images of Ag_2O/TiO_2 with different weight ratio: (a) 8:1, (b) 4:1, (c) 1:4, and (d) 1:8.

increases correspondingly, except for Ag_2O/TiO_2 samples at high weight ratios. For less than 6:1, a few of Ag_2O nanoparticles on TiO_2 nanobelts can be observed, which causes the low photodegradation efficiency. The degradation rate for 8:1 is only 75% in 24 min, although much higher than that of pure TiO_2 nanobelts (25%). The corresponding SEM image of Ag_2O/TiO_2 nanobelts for 8:1 is shown in Figure 7a. From 6:1 to 1:6 of weight ratio, Ag_2O/TiO_2 heterostructure samples all completely degraded 20 mL MO solution under UV light irradiation in 24 min. The results imply that the Ag_2O/TiO_2 heterostructure with a wide weight ratio is easily formed on the interface between Ag_2O nanoparticles and TiO_2 nanobelts, which is beneficial to the electronic transmission. For more than 1:6, the Ag_2O/TiO_2 samples with the high weight ratio of Ag_2O have a low photodegradation efficiency, which decreases with the increase in Ag_2O weight ratio. This is because the TiO_2 nanobelts are coated by too many Ag_2O nanoparticles, and the TiO_2 nanobelts as photocatalyst receive less UV light irradiation. The result is confirmed by SEM image of Ag_2O/TiO_2 with weight ratio of 1:8 (Figure 7d). In Figure 7d, the TiO_2 nanobelts are encapsulated by Ag_2O nanoparticles; meanwhile, many detached Ag_2O nanoparticles are observed because of the large amount of Ag_2O.

The visible-light photocatalytic activity of TiO_2 nanobelts, Ag_2O/TiO_2 heterostructure and Ag_2O nanoparticles is also evaluated by photocatalytic degradation of MO aqueous

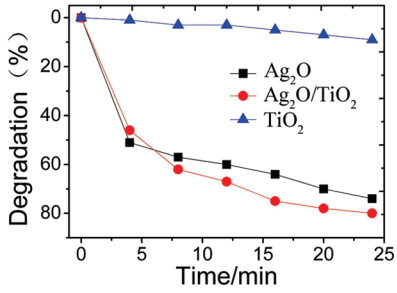

FIGURE 8. Visible-light photocatalytic activity of the TiO_2 nanobelts, Ag_2O/TiO_2 heterostructure (1:1) and Ag_2O nanoparticles.

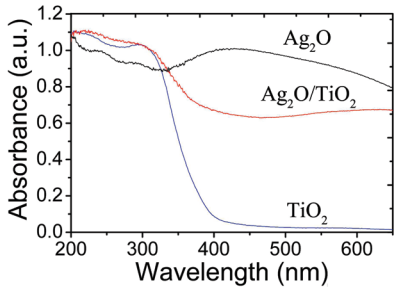

FIGURE 9. UV−vis DRS of TiO_2 nanobelts, Ag_2O/TiO_2 heterostructure, and Ag_2O nanoparticles.

solution under visible-light irradiation, which is shown in Figure 8. Because of the large band gap energy (3.2 eV for anatase), TiO_2 nanobelts photocatalysis proceed only at wavelengths shorter than approximately 400 nm. So, TiO_2 nanobelts have a low photocatalytic activity under visible light, and the degradation is only 9% in 24 min. Surprisingly, we found that the pure Ag_2O nanoparticles have a good visible-light photocatalytic activity, and the corresponding degradation of MO reaches 74% in 24 min. The photocatalytic activity of the Ag_2O/TiO_2 heterostructure is a little better than that of the pure Ag_2O nanoparticles. The corresponding degradation ratio reaches 80%. Because the Ag_2O/TiO_2 composite photocatalyst at the weight ratio of 1:1 has only a half weight of Ag_2O, the visible-light photocatalytic activity of Ag_2O/TiO_2 heterostructure improves apparently when contrasted with pure Ag_2O nanoparticles. So, in TiO_2 nanobelts and Ag_2O nanoparticles, there exist some coordination function, which may be due to the heterostructure effect between them.

The UV−vis DRS of the different samples are shown in Figure 9. TiO_2 nanobelts exhibit a steep absorption edge located at 380 nm. Ag_2O nanoparticles display strong capability of light absorption in both UV and visible light range of 200−650 nm in addition to the intrinsic absorption band derived from the band gap transition, which leads to good visible light photocatalytic activity. The UV−vis spectra of Ag_2O/TiO_2 heterostructure also exhibit a wide visible light absorption band around 400−650 nm and an absorption band in the UV region assignable to the Ti−O bond. In comparison to pure TiO_2 nanobelts, the absorption edge of Ag_2O/TiO_2 heterostructure red-shifts to about 500 nm, and band gap is estimated as 2.4 eV. The absorption above 400 nm in Ag_2O/TiO_2 heterostructure photocatalyst is attributed to the presence of Ag_2O nanoparticles as visible-light sensitization, which has a strong and wide absorption band in the visible-light region.

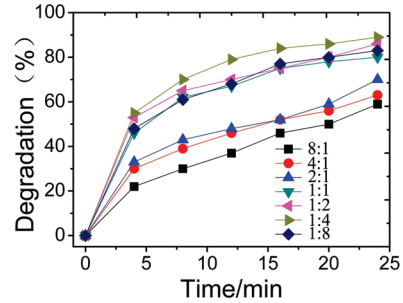

FIGURE 10. Comparison of photocatalytic activities among the Ag_2O/TiO_2 samples with different weight ratio of TiO_2 and Ag_2O under visible-light irradiation in 24 min.

The photocatalytic activities of the Ag_2O/TiO_2 nanobelts with the different Ag_2O content are tested upon visible light irradiation, which is shown in Figure 10. The visible light photocatalytic activity of the Ag_2O/TiO_2 nanobelts increases with an increase in Ag_2O content from 8:1 to 1:4. When the ratio of TiO_2 and Ag_2O reaches at 1:4, the Ag_2O/TiO_2 nanobelts has a highest photocatalytic activity, and the degradation rate is 89% under visible-light irradiation in 24 min. The result is consistent with DRS results, which illuminates that Ag_2O nanoparticles as visible-light sensitization improve the visible-light photocatalytic activity of the Ag_2O/TiO_2 nanobelts. The increase of Ag_2O content obviously enhances the photocatalytic activity of Ag_2O/TiO_2 nanobelts. However, Ag_2O/TiO_2 nanobelts with weight ratio of 1:8 exhibit a little lower the photocatalytic activity than that of 1:4. Meanwhile, Ag_2O/TiO_2 nanobelts with weight ratio of 1:1, 1:2, 1:4, and 1:8 all display a better visible-light photocatalytic activity than that of pure Ag_2O nanoparticles. It is explained that the smaller Ag_2O nanoparticles on TiO_2 nanobelts have a higher activity that is mostly due to Ag_2O/TiO_2 heterostructure with energy band matching.

To investigate the stability of the Ag_2O/TiO_2 heterostructure on photocatalytic activity under UV and visible light irradiation, the same samples were repeatedly used for four times after separation via membrane filtration, and are shown in Figure 11. Regretfully, the Ag_2O/TiO_2 photocatalyst is unstable for repeated use under UV irradiation. The photocatalytic activity of Ag_2O/TiO_2 heterostructure continuously decreases, and the photocatalytic degradation efficiency of MO is only 60% after repeatedly four times for 96 min. However, Ag_2O/TiO_2 photocatalyst exhibits very stable photocatalytic activity under visible-light irradiation as shown in Figure 11B. There is no obvious decrease on the removal rate of MO after four cycles.

To find the above reason, we examined the XRD patterns of the Ag_2O/TiO_2 photocatalyst at the end of the repeated bleaching experiment under UV and visible-light irradiation. As seen from Figure 12 (0), the Ag_2O/TiO_2 sample before UV irradiation is composed of TiO_2 and Ag_2O with good crystallinity. After repeated UV photocatalytic degradation experiments, the peaks corresponding to Ag are detected in the XRD pattern after the first photocatalytic degradation of MO, which is shown in Figure 12 (1). The Ag amount is continu-

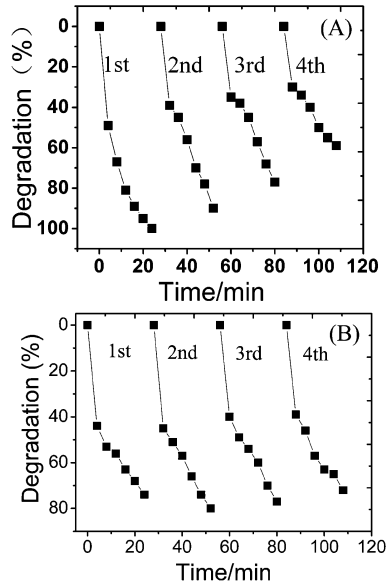

FIGURE 11. Irradiation-time dependence of photocatalytic degradation of MO aqueous solution over Ag_2O/TiO_2 heterostructure during repeated photooxidation experiments under (A) UV and (B) visible-light irradiation.

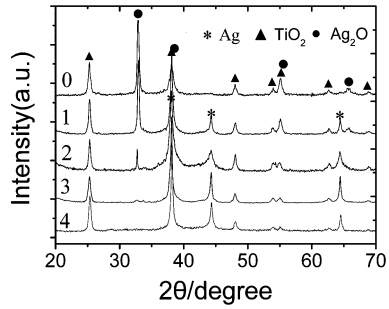

FIGURE 12. XRD patterns of Ag_2O/TiO_2 heterostructure after the repeated photocatalytic degradation experiments for four times under UV-light irradiation.

ally increased with repeated times, and simultaneously, the Ag_2O peaks are continually weakened. After proceeded with the fourth cycle, the Ag_2O peaks almost disappeared (Figure 12 (4)), indicating structural transformation of Ag from Ag_2O phase during UV photocatalytic degradation experiments. We also found the pure Ag_2O nanoparticles are stable under UV irradiation. The results suggest that Ag_2O is destroyed by exposure to UV with the presence of TiO_2. It is possible that the Ag species are obtained from Ag_2O phase by electron reducing action of conduction band of TiO_2 nanobelts under UV irradiation. The XRD results are consistent with the repeated photocatalytic degradation, and the Ag_2O nanoparticles play an important role in improving the photocatalytic activities of Ag_2O/TiO_2 heterostructure. Numerous studies have suggested that fine particles of transition metals or their oxides, when dispersed on the surface of a photocatalyst matrix, can act as electron traps on n-type semiconductors (27, 35). Here, indirect evidence of electron trapping on Ag_2O nanoparticles was demonstrated by the enhanced photocatalytic activity of Ag_2O/TiO_2 heterostructure, compared with pure TiO_2 nanobelts. Direct evidence of photoelectron transfer between the trapping particles and the photocatalyst matrix was demonstrated by XRD results

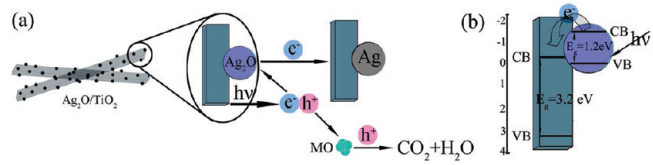

FIGURE 13. Schematic view for electron-hole separations and energy band matching of Ag_2O/TiO_2 heterostructure under (a) UV- and (b) visible-light irradiation.

of Ag_2O/TiO_2 heterostructure after the repeated photocatalytic degradation experiments. In comparison with XRD result under UV-light irradiation, the peak intensity and position of Ag_2O and TiO_2 of Ag_2O/TiO_2 samples under visible-light irradiation maintain basically unchanged with increasing photocatalytic degradation time (the result is given in the paper), which imply that the reaction mechanism under visible-light irradiation is different from that under UV-light irradiation.

The Ag_2O/TiO_2 heterostructure rapid precipitation process is presented, which is shown in Supporting Information 2. The Ag_2O as a purifying agent is usually used for adsorption and removal of suspended small particles in the polluted water. Here, we confirm that the Ag_2O nanoparticles themselves have excessive negative charges (zeta potential is about −31.24 mV), which easily adsorb on TiO_2 nanobelts with positive charges, forming the heterostructure between Ag_2O nanoparticles and TiO_2 nanobelts. Conventional powder photocatalysts, such as P-25, have a serious limitation the need for post-treatment separation in a slurry system (22). Titanate nanobelts with large aspect ratio can be separated easily from the solution, which overcomes the disadvantages of the spherical TiO_2 catalysts. However, the pure TiO_2 nanobelts also need complicated process and long recovery time. The rapid precipitation of Ag_2O/TiO_2 heterostructure occurs in the first one min of the experiment setup, and forms a gray layer at bottom. Correspondingly, pure TiO_2 nanobelts show colloidal suspension as control for about one hour. For P-25, the "milky" look of the suspension is stable for over 48 h. So, the Ag_2O/TiO_2 photocatalyst is easily recovered after repeated photocatalytic degradation, which creates advantageous conditions for repeat utilization.

To fully understand the loading effects by Ag_2O nanoparticles on TiO_2 nanobelts, it is necessary to obtain further information about the energy band of Ag_2O and TiO_2. On the basis of above results, a possible mechanism of high photocatalytic activities of Ag_2O/TiO_2 heterostructure under UV- and visible-light irradiation is shown in Figure 13. Meanwhile, the relevant formula reactions are shown as following

$$TiO_2 \xrightarrow{h\nu} h^+ + e^- \qquad (1)$$

$$Ag_2O \xrightarrow{h\nu} h^+ + e^- \quad (2)$$

$$Ag_2O + e^- \rightarrow Ag + O_2 \quad (3)$$

$$h^+ + H_2O \rightarrow \bullet OH + H^+ \quad (4)$$

$$e^- + O_2 + H_2O \rightarrow \bullet OH + OH^- \quad (5)$$

Under UV-light irradiation, both TiO_2 nanobelts and Ag_2O nanoparticles are excited to produced h^+ and e^- according to formula 1 and 2. The generated electrons and holes in TiO_2 and Ag_2O react with H_2O and produce reactive oxygen species · OH followed by formula 4 and 5. Under normal case, most of electrons-holes pairs recombine rapidly, the pure TiO_2 nanobelts have a low photocatalytic activity. Herein, Ag_2O nanoparticles on the surface of TiO_2 nanobelts capture electrons effectively. Simultaneously, the heterostructure between Ag_2O nanoparticles and TiO_2 nanobelts is beneficial to electrons transmission from TiO_2 nanobelts to Ag_2O nanoparticles. The obtained e^- reacts with Ag_2O nanoparticles, which is reduced to Ag according to formula 3. Formula 3 is confirmed by XRD result obtained by repeated experiment under UV light irradiation (Figure 12). The Ag_2O nanoparticles as electron absorbent prevent electrons and holes from recombination, and the holes efficiently oxidize organic compounds, and thus the photocatalytic reaction is enhanced greatly. At the same time, the generated O_2 from Ag_2O-loaded photocatalysts according to formula 3 promote reaction 5 to produce more reactive oxygen species · OH, which also improve the photocatalytic activity under UV-light irradiation. So, the enhancement of UV photocatalytic activity of Ag_2O/TiO_2 heterostructure is based on the improvement of quantum efficiency cause by a sacrifice of Ag_2O.

Under visible -light irradiation, only Ag_2O due to the narrower band gap (1.3 eV) (36) can be excited to produce h^+ and e^- according to formula 2, and then formula 4 and 5 are. However, the Ag_2O/TiO_2 heterostructure has a higher photocatalytic activity than that of pure TiO_2 nanobelts and Ag_2O nanoparticles. The result is mostly attributed to the heterostructure and energy band match of Ag_2O nanoparticles and TiO_2 nanobelts. The migration of photogenerated carriers is promoted because less of a barrier exists between Ag_2O/TiO_2 heterostructure. Meanwhile, this transfer process is thermodynamicly favorable because of both the conduction band and valence band of Ag_2O (CB, −2.0, and VB, −0.7 V, vs NHE at pH 12.0) lie above that of TiO_2 (CB, −0.8, and VB, 2.4 V, vs NHE at pH 12.0) (32, 33, 36), which is shown in Figure 13b. The lifetime of the excited electrons and holes then is prolonged in the transfer process, inducing higher quantum efficiency. Therefore, the probability of electron and hole recombination is reduced, a larger number of electrons concentrate on TiO_2 nanobelts, and holes locate on the Ag_2O nanoparticles, which participates in photocatalytic reactions to decompose organic pollution, and thus the photocatalytic reaction is enhanced greatly.

Although the enhancement mechanisms of Ag_2O/TiO_2 photocatalyst under UV- and visible-light irradiation are different, the heterostructure of Ag_2O/TiO_2 is the primary reason for the enhancement. Ag_2O nanoparticles are unsteady under UV-light irradiation in the existence of electrons from TiO_2, which has a strong reducing property. Thus, the Ag_2O/TiO_2 photocatalyst has a bad cyclic stability under UV-light irradiation. It is very well-known that the Ag nanoparticles are easy to be slowly oxidized in the moist environment (37, 38) and be quickly oxidized by heating at the high oxygen pressure environment. A simply and practical method for the recycle of Ag_2O needs to be found. Possibly, a steady system based on multiphase heterostructures, such as $Ag/Ag_2O/TiO_2$ (19) or photoelectrocatalysis with Ag_2O as an anode modified by TiO_2, should be carried out. The related works are proceeding.

CONCLUSIONS

Ag_2O/TiO_2 nanobelts heterostructure were prepared by chemical precipitating Ag_2O nanoparticles on TiO_2 nanobelts, and microstructure was characterized by SEM and HRTEM. The Ag_2O/TiO_2 nanobelts with heterostructure was a novel photocatalyst with high activity driven both UV and visible light for the degradation of MO. The results of XRD, PL, and DRS demonstrated the two different mechanisms of the photocatalytic activity under UV and visible light, respectively. Under UV-light irradiation, Ag_2O nanoparticles as an electron absorbing agent scavenged the valence electrons of TiO_2 nanobelts to enhance electron-hole separation. The valence hole of TiO_2 nanobelts became trapped OH group on the surface to produce •OH radicals. Under visible-light irradiation, Ag_2O nanoparticles on TiO_2 nanobelts as visible-light active component enhanced Ag_2O/TiO_2 heterostructure photocatalytic activity via the synergetic effects on the thermocatalyticly activity and the efficient electron transmission at the Ag_2O/TiO_2 interface. So, photocatalysts modified by some metal oxides with electron capture and visible-light sensitization capability, such as Ag_2O, W_2O_3, NiO, and PdO, to form heterostructures will be an effective method to improve photocatalytic activity.

Acknowledgment. This research was supported by an NSFC (NSFDYS: 50925205, 50872070, 50702031, Grant 50990303, IRG: 50721002), and the Program of Introducing Talents of Discipline to Universities in China (111 Program b06015)).

Supporting Information Available: Additional figures (PDF). This material is available free of charge via the Internet at http://pubs.acs.org.

REFERENCES AND NOTES

(1) Fujishima, A.; Honda, K. *Nature* **1972**, *238*, 37.
(2) Muruganandham, M.; Swaminathan, M. *Dyes Pigm.* **2006**, *68*, 133.
(3) Tan, L. K.; Kumar, M. K.; An, W. W.; Gao, H. *ACS Appl. Mater. Interfaces* **2010**, *2*, 498.

(4) Fei, H. L.; Liu, Y. P.; Li, Y. P.; Sun, P. C.; Yuan, Z. Z.; Li, B. H.; Ding, D. T.; Chen, T. H. *Microporous Mesoporous Mater.* **2007**, *102*, 318.
(5) Park, J. H.; Kim, S.; Bard, A. J. *Nano Lett.* **2006**, *6*, 24.
(6) Formo, E.; Lee, E.; Campbell, D.; Xia, Y. *Nano lett.* **2008**, *8*, 668.
(7) Chien, S. H.; Liou, Y. C.; Kuo, M. *Synth. Met.* **2005**, *152*, 333.
(8) Tung, W. S.; Daoud, W. A. *ACS Appl. Mater. Interfaces* **2009**, *1*, 2453.
(9) Huang, L.; Peng, F.; Wang, H. J.; Yu, H.; Li, Z. *Catal. Commun.* **2009**, *10*, 1839.
(10) Li, Q.; Page, M. A.; Marinas, B. J.; Shang, J. K. *Environ. Sci. Technol.* **2008**, *42*, 6148.
(11) Yang, S. G.; Liu, Y. Z.; Sun, C. *Appl. Catal., A* **2006**, *301*, 284.
(12) Wang, J.; Tafen, D. N.; Lewis, J. P.; Hong, Z. L.; Manivannan, A.; Zhi, M. J.; Li, M.; Wu, N. Q. *J. Am. Chem. Soc.* **2009**, *131*, 12290.
(13) Maeda, K.; Shimodaira, Y.; Lee, B.; Teramura, K.; Lu, D.; Kobayashi, H.; Domen, K. *J. Phys. Chem. C* **2007**, *111* (49), 18264.
(14) Štengl, V.; Houšková, V.; Bakardjieva, S.; Murafa, N. *ACS Appl. Mater. Interfaces* **2010**, *2* (2), 575.
(15) Zhang, J.; Pan, C. X.; Fang, P. F.; Wei, J. H.; Xiong, R. *ACS Appl. Mater. Interfaces* **2010**, *2* (4), 1173.
(16) Zhao, W.; Chen, C.; Li, X.; Zhao, J. *J. Phys. Chem. B* **2002**, *106*, 5022.
(17) Bae, E.; Coi, W. *Environ. Sci. Technol.* **2003**, *37*, 147.
(18) Hu, C.; Hu, X. X.; Wang, L. S.; Qu, J. H.; Wang, A. M. *Environ. Sci. Technol.* **2006**, *40*, 7903.
(19) Hu, C.; Lan, Y. Q.; Qu, J. H.; Hu, X. X.; Wang, A. M. *J. Phys. Chem. B* **2006**, *110*, 4066.
(20) Moon, J.; Yun, C. Y.; Chung, K. W.; Kang, M. S.; Yi, J. *Catal. Today* **2003**, *87* (1−4), 77.
(21) Zhang, Y. G.; Ma, L. L.; Li, J. L.; Yu, Y. *Environ. Sci. Technol.* **2007**, *41* (17), 6264.
(22) Blumberg, I.; Starosvetsky, J.; Bilanovic, D.; Armon, R. *J. Colloid Interface Sci.* **2009**, *336*, 107.
(23) Zhu, H. Y.; Gao, X. P.; Lan, Y.; Song, D. Y.; Xi, Y. X.; Zhao, J. C. *J. Am. Chem. Soc.* **2004**, *126*, 8380.
(24) Zhu, H. Y.; Orthman, J.; Li, J. Y.; Zhao, J. C.; Churchman, G. J.; Vansant, E. F. *Chem. Mater.* **2002**, *14*, 5037.
(25) Zhang, X.; Yang, H.; Zhang, F.; Chan, K. Y. *Mater. Lett.* **2006**, *61*, 2231.
(26) Arabatzis, I. M.; Stergiopoulos, T.; Andreeva, D.; Kitova, S.; Neophytides, S. G.; Falaras, P. *J. Catal.* **2003**, *220*, 127.
(27) Li, Q.; Xie, R. C.; Mintz, E. A.; Shang, J. K. *J. Am. Ceram. Soc.* **2007**, *90*, 3863.
(28) Korosi, L.; Papp, S.; Menesi, J.; Illes, E.; Zollmer, V.; Richardt, A.; Dekany, I. *Colloids Surf., A* **2008**, *319*, 136.
(29) Zhang, F.; Jin, R.; Chen, J.; Shao, C.; Gao, W.; Li, L.; Guan, N. *J. Catal.* **2005**, *232*, 424.
(30) Sobana, N.; Muruganadham1, M.; Swaminathan, M. *J. Mol. Catal. A* **2006**, *258*, 124.
(31) Xin, B. F.; Jing, L. Q.; Ren, Z. Y.; Wang, B. Q.; Fu, H. G. *J. Phys. Chem. B* **2005**, *109*, 2805.
(32) Priya, R.; Baiju, K. V.; Shukla, S.; BijuÆ, S.; Reddy, M. L. P.; Patil, K. R.; Warrier, K. G. K. *Catal. Lett.* **2009**, *128*, 137.
(33) Priya, R.; Baiju, K. V.; Shukla, S.; Biju, S.; Reddy, M. L. P.; Patil, K.; Warrier, K. G. K. *J. Phys. Chem. C* **2009**, *113*, 6243.
(34) Zou, J.; Xu, Y.; Hou, B.; Wu, D.; Sun, Y. H. *Powder Technol.* **2008**, *183*, 122.
(35) Subramanian, V.; Wolf, E.; Kamat, P. V. *J. Phys. Chem. B* **2001**, *105*, 11439.
(36) Damm, C.; Herrmann, R.; Israel, G.; M|Aauller, F. W. *Dyes Pigm.* **2007**, *74*, 335.
(37) Hu, J. L.; Wang, L.; Cai, W. P.; Li, Y.; Zeng, H. B.; Zhao, L. Q.; Liu, P. S. *J. Phys. Chem. C* **2009**, *113*, 19039.
(38) Deng, H.; Yang, D.; Chen, B.; Lin, C. W. *Sens. Actuators, B* **2008**, *134*, 502.

AM100394X